PHYSICAL REVIEW D, VOLUME 58, 111101

Search for muonic decays of the antiproton at the Fermilab Antiproton Accumulator

M. Hu and G. R. Snow*
University of Nebraska, Lincoln, Nebraska 68588

S. Geer, J. Marriner, M. Martens, R. E. Ray, J. Streets, and W. Wester
Fermi National Accelerator Laboratory, Batavia, Illinois 60510

T. Armstrong
Pennsylvania State University, University Park, Pennsylvania 16802

C. Buchanan, B. Corbin, M. Lindgren, and T. Muller†
University of California at Los Angeles, Los Angeles, California 90024

R. Gustafson
University of Michigan, Ann Arbor, Michigan 48109

(The APEX Collaboration)
(Received 10 August 1998; published 4 November 1998)

A search for antiproton decay has been made at the Fermilab Antiproton Accumulator. Limits are placed on six antiproton decay modes which contain a final-state muon. At the 90% C.L. we find that $\tau_{\bar{p}}/B(\bar{p}\to\mu^-\gamma)>5.0\times10^4$ yr, $\tau_{\bar{p}}/B(\bar{p}\to\mu^-\pi^0)>4.8\times10^4$ yr, $\tau_{\bar{p}}/B(\bar{p}\to\mu^-\eta)>7.9\times10^3$ yr, $\tau_{\bar{p}}/B(\bar{p}\to\mu^-\gamma\gamma)>2.3\times10^4$ yr, $\tau_{\bar{p}}/B(\bar{p}\to\mu^-K_S^0)>4.3\times10^3$ yr, and $\tau_{\bar{p}}/B(\bar{p}\to\mu^-K_L^0)>6.5\times10^3$ yr. [S0556-2821(98)50223-8]

PACS number(s): 13.30.Ce, 11.30.Er, 11.30.Fs, 14.20.Dh

The CPT theorem requires that the proton and antiproton ($\bar{p}$) lifetimes are equal. Searches for proton decay have yielded lower limits on the proton lifetime $\tau_p>O(10^{32})$ yr [1]. A search for $\bar{p}$ decay with a short lifetime ($\tau_{\bar{p}}\ll\tau_p$) tests both the CPT theorem and the intrinsic stability of antimatter.

Currently, the most stringent lower limits on $\tau_{\bar{p}}$ can, in principle, be obtained from a comparison of recent measurements of the cosmic ray antiproton flux with predictions based on expectations for secondary production of antiprotons in the interstellar medium. The agreement between the observed and predicted rates implies that $\tau_{\bar{p}}$ is not small compared to T/γ, where T is the $\bar{p}$ confinement time within the galaxy ($\sim10^7$ yr) and γ is the Lorentz factor for the observed antiprotons. However, to extract a limit on $\tau_{\bar{p}}$ requires careful consideration of the relationship between the interstellar $\bar{p}$ flux and the flux observed at the Earth, and an adequate estimate of the systematic uncertainties on the predictions. These calculations are expected to yield a limit of about 10^6 yr [2]. This indirect limit would not be valid if current models of $\bar{p}$ production, propagation, and interaction in the interstellar medium are seriously flawed by, for example, our lack of knowledge of the nature of most of the matter in the galaxy.

Laboratory searches for $\bar{p}$ decay have so far provided less stringent limits on $\tau_{\bar{p}}$. However, these limits do not suffer from large model dependent uncertainties. The most stringent published laboratory limits on $\bar{p}$ decay have been obtained from (a) measurements of the containment lifetime of ~1000 antiprotons stored in an ion trap, yielding [3] $\tau_{\bar{p}}>3.4$ months, and (b) prior searches at the Fermilab antiproton accumulator for explicit $\bar{p}$ decay modes with an electron in the final state, yielding [4] $\tau_{\bar{p}}/B(\bar{p}\to e^-\gamma)>1848$ yr, $\tau_{\bar{p}}/B(\bar{p}\to e^-\pi^0)>554$ yr, $\tau_{\bar{p}}/B(\bar{p}\to e^-\eta)>171$ yr, $\tau_{\bar{p}}/B(\bar{p}\to e^-K_S^0)>29$ yr, and $\tau_{\bar{p}}/B(\bar{p}\to e^-K_L^0)>9$ yr.

Angular momentum conservation requires that a decaying $\bar{p}$ would produce a fermion (electron, muon, or neutrino) in the final state. In this paper we report results from the first search for antiproton decay modes with a muon in the final state. The results have been obtained using the APEX detector at the Fermilab Antiproton Accumulator. The experiment was designed to search for decay modes with an electron or muon in the final state; only the muon results are presented here.

A full description of the APEX detector can be found in Ref. [5]. In the following we give a brief description of the main detector components relevant to the analysis described in this paper. A schematic of the APEX detector is shown in Fig. 1. The detector, which was located in a straight section of the Accumulator ring, consisted of: (i) A 3.7 m long evacuated decay tank operated at 10^{-11} Torr. The downstream section of the tank consists of a 96 cm diameter cylinder with a 1.2 mm thick stainless steel window. (ii) A movable tungsten wire target at the upstream end of the tank ($z=0$, where in the APEX co-ordinate system z is measured in the direction of the antiproton beam). The target could be inserted into the beam halo to produce a localized source of particles for aligning and calibrating the detector. (iii) Hori-

*Corresponding author. Email address: gsnow@unlhep.unl.edu
†Present address: Universität Karlsruhe, 76128 Karlsruhe, Germany.

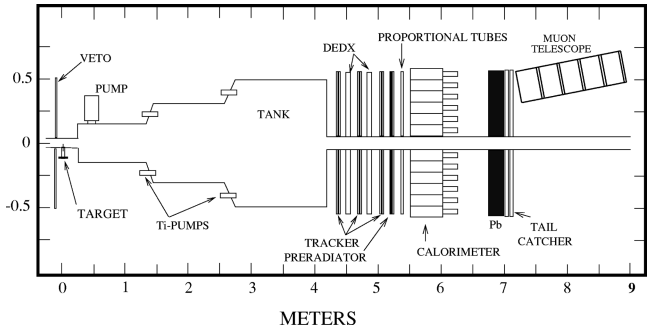

FIG. 1. Schematic of the APEX detector.

zontal and vertical scintillation counters arranged around the 10 cm diameter beam pipe immediately upstream of the tank and target. The counters covered a $1\times1\ \mathrm{m}^2$ area normal to the beam direction, and were used to veto tracks from upstream interactions. (iv) Three planes of horizontal and three planes of vertical scintillation counters downstream of the tank. The last planes of horizontal and vertical counters were downstream of a 2.3 radiation length lead wall, providing a preradiator to aid in identifying electrons and photons. The remaining counter planes were upstream of the lead, and provided pulse height information used to count the number of charged particles in an event (dE/dx counters). (v) Three planes of horizontal and three planes of vertical 2 mm diameter scintillating fibers downstream of the tank and upstream of the preradiator lead. These detectors were used for tracking, and provided three space points along the track trajectory with typical residuals of 620 μm in the directions transverse to the beam direction. This enabled the origin of tracks emerging from the decay tank to be located with a precision $\sigma_z\sim13$ cm along the beam orbit. The measured average single-hit efficiency for the tracker planes is $(89.2\pm1.5)\%$ for tracks in the event samples described in this paper. The measured track reconstruction efficiency, based on a sample of events that are consistent with having one minimum-ionizing particle passing through the dE/dx and muon telescope (see below) counters, is $(90\pm7)\%$. (vi) A lead-scintillator sampling electromagnetic calorimeter [6] constructed from 144 rectangular $10\times10\ \mathrm{cm}^2$ modules that are 14.7 radiation lengths deep. The modules were arranged in a 13×13 array with 6 modules removed from each of the four corners, and the central module removed to allow passage of the beam pipe. The calorimeter was calibrated by measuring the response to minimum ionizing tracks and reconstructing $\pi^0\rightarrow\gamma\gamma$ and $\eta\rightarrow\gamma\gamma$ mass peaks using data samples recorded with the calibration target inserted in the beam halo. The measured mass peaks had fractional r.m.s. widths given by $\sigma_m/\mathrm{m}\sim0.25$ for cluster pairs in the energy range of interest for the experiment. This mass resolution is dominated by the energy resolution of the calorimeter. (vii) A tail catcher (TC) downstream of the calorimeter consisting of a 20 cm deep lead wall followed by planes of horizontal and vertical scintillation counters. (viii) A limited-acceptance muon telescope (MT), 10 nuclear interaction lengths deep, located downstream of the TC, and aligned to point towards the center of the decay tank. The MT consists of a sandwich of five iron plates and five $30\times30\ \mathrm{cm}^2$ scintillation counters.

The APEX experiment took data when there were typically 10^{12} antiprotons circulating in the 474 m circumference accumulator ring operating with a central $\bar{p}$ momentum of 8.90 ± 0.01 GeV/c ($\gamma=9.54\pm0.01$). A measure of the sensitivity of the APEX data sample is given by:

$$S\equiv\frac{1}{\gamma}\int N_{\bar{p}}(t)\,dt=(3.31\pm0.03)\times10^9\ \mathrm{yr},$$

where $N_{\bar{p}}(t)$ is the number of circulating antiprotons at time t, the integral is over the live-time of the experiment, and the uncertainty arises from the precision with which the time dependent beam current was recorded.

To search for muonic $\bar{p}$ decays occurring as the beam particles traverse the decay tank, data were recorded with a muon trigger that required a coincidence between at least two of the five MT scintillation counters. These triggers were eliminated if they were in coincidence with a signal in one or more of the upstream veto counters indicating the presence of an interaction upstream of the decay tank. This loose trigger resulted in 1.2×10^6 events being recorded. These events predominantly arise from interactions of the $\bar{p}$ beam with the residual gas in the decay tank or with material surrounding the beam. The coincident MT counter signals are then produced by traversing muons coming from charged pion decays, and by hadronic showers not contained in the calorimeter and TC.

Off-line, after final calibration of the scintillation counters, the upstream veto counter requirement was reapplied using a more stringent threshold. This reduced the data sample to 1.1×10^6 events. Further requirements were then imposed to select events containing a candidate energetic muon that traverses the MT and originates from within the decay tank. These requirements were (i) that at least four of the five MT counters be above threshold (4.2×10^4 events), and (ii) the presence of one and only one scintillating fiber track that extrapolates to the MT counters within the expected uncertainty due to multiple scattering, and also extrapolates back to the beam orbit with a point of closest approach within the fiducial volume of the decay tank ($0<z<375$ cm) and with an impact parameter less than 1 cm (416 events).

To further suppress backgrounds, additional requirements can be imposed on the event topology and kinematics. We begin by considering the process $\bar{p}\rightarrow\mu^-\gamma$, which would result in events in which an energetic photon is produced coplanar with the muon (i.e., traveling within the plane defined by the muon and the incoming beam direction). After requiring at least one neutral cluster [5] in the calorimeter (209 events) that is coplanar with the muon candidate ($\pm5°$), the data sample is reduced to 14 events. The observed neutral cluster energy distribution for these events is compared in Fig. 2 with the predicted distribution obtained using the GEANT [7] simulation described below, and corresponding to $\bar{p}\rightarrow\mu^-\gamma$ decay with a lifetime $\tau_{\bar{p}}/B(\bar{p}\rightarrow\mu^-\gamma)=5000$ yr. The observed distribution peaks at low cluster energies, with a tail extending to approximately 2 GeV. In contrast, the predicted distribution for $\bar{p}\rightarrow\mu^-\gamma$ decays peaks at about 3.5 GeV, with only 4.4% of the simulated events having cluster

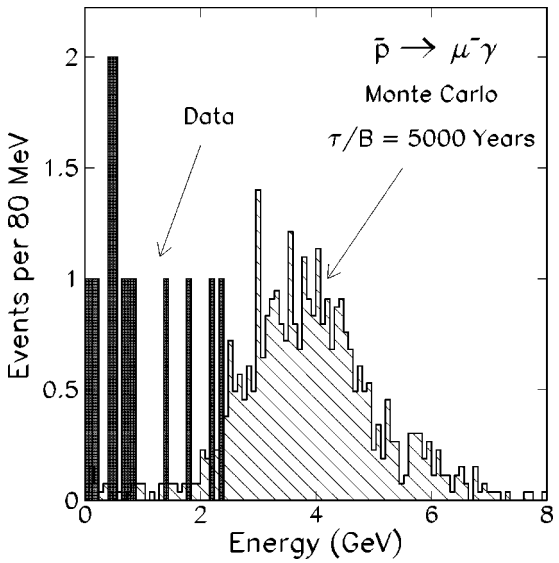

FIG. 2. Distribution of neutral cluster energies for the 14 events that pass the $\bar{p}\rightarrow\mu^-\gamma$ selection criteria described in the text (dark histogram) compared with the predicted distribution for a signal corresponding to $\tau_{\bar{p}}/B=5000$ yr (hatched histogram). Limits are based on the region $E>3$ GeV.

energies less than 2 GeV. We conclude that there is no evidence for a signal. To eliminate the background, we therefore require that the neutral cluster energy exceed a minimum value E_{min}, and choose $E_{min}=3$ GeV. No candidate events remain. We note that although the choice of E_{min} is somewhat arbitrary, the final limit that we obtain on the decay $\bar{p}\rightarrow\mu^-\gamma$ is not very sensitive to small changes in E_{min}. The resulting limit on $\tau_{\bar{p}}/B(\bar{p}\rightarrow\mu^-\gamma)$ is given in years by

$$\tau_{\bar{p}}/B(\bar{p}\rightarrow\mu^-\gamma)>\frac{\epsilon}{\gamma}\frac{1}{N_{max}}\int N_{\bar{p}}(t)dt$$

$$=(3.31\pm0.03)\times10^9\frac{\epsilon}{N_{max}}, \qquad (1)$$

where $N_{max}=2.3$ is the 90% C.L. upper limit on the observation of $N=0$ events, and ϵ is the fraction of decays taking place uniformly around the accumulator ring that would pass the trigger and event selection requirements. To take account of σ_ϵ, the systematic uncertainty on ϵ, we use the prescription given in Ref. [8], giving, at 90% C.L.

$$N_{max}=2.3\times(1+2.3\sigma_r^2/2), \qquad (2)$$

where $\sigma_r\equiv\sigma_\epsilon/\epsilon$.

The GEANT Monte Carlo program has been used to simulate the detector response and calculate ϵ. The detector simulation includes a full description of the detector geometry, and correctly describes the calorimeter, tracker, and relevant scintillation counter responses (dE/dx, MT) measured using calibration data, together with the measured performance of the muon trigger. Further details can be found in Ref. [5]. The efficiency ϵ was obtained by generating $10^5\bar{p}\rightarrow\mu^-\gamma$ decays uniformly along the beam orbit within the decay tank. To a good approximation, the geometrical efficiency of the detector and trigger is negligible for decays occurring outside of the tank. We obtain $\epsilon=(3.7\pm0.9)\times10^{-5}$, where the uncertainty on ϵ arises from the systematic uncertainties on the trigger calibration, calorimeter energy scale, and track efficiency. The trigger and calorimeter scale uncertainties yield contributions to σ_ϵ of $\pm18\%$ and $\pm15\%$, respectively, and have been evaluated by analyzing GEANT Monte Carlo $\bar{p}\rightarrow\mu^-\gamma$ samples in which the simulated trigger and calorimeter scales have been changed by $\pm1\sigma$. The overall systematic uncertainty on ϵ has been calculated by adding these contributions in quadrature with the uncertainty on the track efficiency ($\pm7\%$). Inserting the calculated ϵ and σ_ϵ into Eqs. (1) and (2), we obtain the result $\tau_{\bar{p}}/B(\bar{p}\rightarrow\mu^-\gamma)>5.0\times10^4$ yr (90% C.L.).

Now consider the two-body decays $\bar{p}\rightarrow\mu^-\pi^0$ and $\bar{p}\rightarrow\mu^-\eta$ (with π^0, $\eta\rightarrow\gamma\gamma$), and the three-body decay $\bar{p}\rightarrow\mu^-\gamma\gamma$. These decays would result in events with one or two neutral clusters observed in the calorimeter, where the one-cluster events occur when the two photon-showers are not spatially resolved in the calorimeter or when one of the photons is outside of the calorimeter acceptance. In addition, the η may also decay into more complicated final states producing further clusters in the calorimeter. To optimize the search for $\mu^-\pi^0$ and $\mu^-\eta$ final states, we divide the 209 events described previously that have a muon candidate plus one or more neutral clusters into two subsamples, namely a one-cluster sample containing 104 events, and a multicluster sample containing 105 events. The clusters in the one-cluster sample are required to be coplanar with the muon ($\pm10°$), and the cluster-pairs formed by the two highest energy clusters in the multicluster events are also required to be coplanar with the muon ($\pm10°$). These requirements reduce the samples to 13 one-cluster and 10 multicluster events. We next require that the multicluster events, which would contain two photons if they were genuine $\bar{p}\rightarrow\mu^-\pi^0$, $\mu^-\eta$, or $\mu^-\gamma\gamma$ decays, have a preradiator signal above a threshold ($0.5\times$minimum-ionizing pulse height) consistent with either one or both photons converting in the preradiator lead. Only three multicluster events satisfy this requirement. Hence, we are left with 16 events with $\geqslant1$ cluster ($\mu+\geqslant1$ cluster) for further analysis.

Under the hypothesis that the observed ($\mu\gamma$) and ($\mu\gamma\gamma$) systems arise from the decay of a beam particle, the mass of the parent particle can be computed from the measured muon direction and the directions and energies of the neutral clusters, using the constraint that the vector sum of the momentum components of the daughter particles transverse to the beam direction is zero. The resulting mass distribution for the remaining 16 ($\mu+\geqslant1$ cluster) events is compared in Fig. 3 with predictions from the GEANT simulation for the decays (a) $\bar{p}\rightarrow\mu^-\pi^0$, (b) $\bar{p}\rightarrow\mu^-\eta$, and (c) $\bar{p}\rightarrow\mu^-\gamma\gamma$. The observed mass distribution peaks at low masses with a tail extending to approximately 0.7 GeV/c^2. In contrast to this, the simulated signal distributions peak at the $\bar{p}$ mass, with only 17% (23%) [13%] of the simulated $\mu^-\pi^0$ ($\mu^-\eta$) [$\mu^-\gamma\gamma$] decays resulting in reconstructed masses less than 0.7 GeV/c^2. We conclude that there is no evidence for a signal. To eliminate the background, we therefore require that the reconstructed mass exceed a minimum value m_{min},

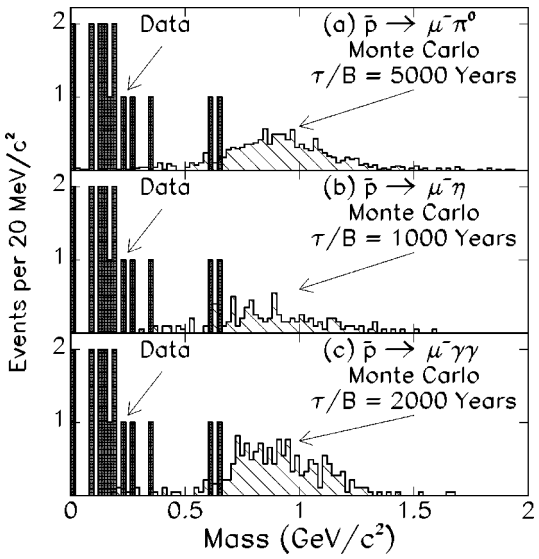

FIG. 3. Distribution of event masses for the 16 events that pass the selection criteria described in the text (dark histograms) compared with predictions from a GEANT simulation (hatched histograms) for the decays (a) $\bar{p} \rightarrow \mu^- \pi^0$, (b) $\bar{p} \rightarrow \mu^- \eta$, and (c) $\bar{p} \rightarrow \mu^- \gamma\gamma$. The two entries in the lowest bin are events with calorimeter energy less than the π^0 rest energy. The predicted signal distributions are normalized to correspond to $\tau_{\bar{p}}/B = 5000$ yr for the $\mu^- \pi^0$ mode, 1000 yr for the $\mu^- \eta$ mode, and 2000 yr for the $\mu^- \gamma\gamma$ mode. Limits are based on the region Mass >0.75 GeV.

and choose $m_{min} = 0.75$ GeV/c^2. No candidate events remain. We note that although the choice of m_{min} is somewhat arbitrary, the final limits that we obtain on the decays $\bar{p} \rightarrow \mu^- \pi^0$, $\mu^- \eta$, and $\mu^- \gamma\gamma$ are not very sensitive to small changes in m_{min}. The calculated overall efficiencies ϵ for these decays to pass our trigger and analysis requirements are $(3.6 \pm 0.9) \times 10^{-5}$ for the $\mu^- \pi^0$ mode, $(6.1 \pm 1.9) \times 10^{-6}$ for the $\mu^- \eta$ mode, and $(1.8 \pm 0.5) \times 10^{-5}$ for the $\mu^- \gamma\gamma$ mode. Substituting the values into Eqs. (1) and (2) yields the limits $\tau_{\bar{p}}/B(\bar{p} \rightarrow \mu^- \pi^0) > 4.8 \times 10^4$ yr, $\tau_{\bar{p}}/B(\bar{p} \rightarrow \mu^- \eta) > 7.9 \times 10^3$ yr at 90% C.L., and $\tau_{\bar{p}}/B(\bar{p} \rightarrow \mu^- \gamma\gamma) > 2.3 \times 10^4$ yr at 90% C.L.

TABLE I. Summary of lifetime limits for $\bar{p}$ decay to six muonic final states with calculated efficiencies ϵ for each mode.

Decay mode	ϵ	τ/B Limit (yr) (90% C.L.)
$\mu^- + \gamma$	$(3.7 \pm 0.9) \times 10^{-5}$	$>5.0 \times 10^4$
$\mu^- + \pi^0$	$(3.6 \pm 0.9) \times 10^{-5}$	$>4.8 \times 10^4$
$\mu^- + \eta$	$(6.1 \pm 1.9) \times 10^{-6}$	$>7.9 \times 10^3$
$\mu^- + \gamma\gamma$	$(1.8 \pm 0.5) \times 10^{-5}$	$>2.3 \times 10^4$
$\mu^- + K_S^0$	$(3.3 \pm 1.0) \times 10^{-6}$	$>4.3 \times 10^3$
$\mu^- + K_L^0$	$(5.0 \pm 1.5) \times 10^{-6}$	$>6.5 \times 10^3$

Now consider the other possible two-body muonic decay modes of the antiproton, namely decays into the final states $\mu^- K_S^0$, $\mu^- K_L^0$, $\mu^- \rho^0$, and $\mu^- \omega$. Detailed GEANT simulations have been made for these decay modes. The muons from the $\mu^- \rho^0$ and $\mu^- \omega$ decay modes are predicted to have energies that are too low to penetrate the muon telescope. We therefore restrict ourselves to the $\mu^- K_S^0$ and $\mu^- K_L^0$ modes. The calculated efficiencies ϵ for these decays to satisfy the trigger and either the $\mu^- \gamma$ or $\mu^- \pi^0$ search criteria described previously are $(3.3 \pm 1.0) \times 10^{-6}$ for the $\mu^- K_S^0$ mode, and $(5.0 \pm 1.5) \times 10^{-6}$ for the $\mu^- K_L^0$ mode. Substituting these values into Eqs. (1) and (2) yields the limits $\tau_{\bar{p}}/B(\bar{p} \rightarrow \mu^- K_S^0) > 4.3 \times 10^3$ yr and $\tau_{\bar{p}}/B(\bar{p} \rightarrow \mu^- K_L^0) > 6.5 \times 10^3$ yr at 90% C.L.

Finally, our results for the six muonic decay modes presented in this paper are summarized in Table I, and a more comprehensive description of the analysis can be found in Ref. [9].

The APEX experiment was performed at the Fermi National Accelerator Laboratory, which is operated by Universities Research Association, under Contract No. DE-AC02-76CH03000 with the U.S. Department of Energy.

[1] Particle Data Group, R. M. Barnett *et al.*, Phys. Rev. D **54**, 1 (1996) and 1997 off-year partial update for the 1998 edition available on the PDG WWW pages (URL: http://pdg.lbl.gov/).
[2] S. Geer and D. Kennedy, ''The cosmic-ray antiproton spectrum and a limit on the antiproton lifetime,'' astro-ph/9809101.
[3] G. Gabrielse *et al.*, Phys. Rev. Lett. **65**, 1317 (1990).
[4] S. Geer *et al.*, Phys. Rev. Lett. **72**, 1596 (1994).
[5] APEX Collaboration, T. Armstrong *et al.*, Nucl. Instrum. Methods Phys. Res. A **411**, 210 (1998).
[6] M. A. Hasan *et al.*, Nucl. Instrum. Methods Phys. Res. A **295**, 73 (1990).
[7] GEANT Version 3.21, R. Brun *et al.*, CERN Program Library.
[8] R. Cousins and V. Highland, Nucl. Instrum. Methods Phys. Res. A **320**, 331 (1992).
[9] M. Hu, Ph.D. thesis, University of Nebraska, 1998.